

## ZnO quantum dot phosphors converted white light emitting diode

M. Kumar <sup>a</sup>, P. K. Jindal <sup>b</sup>, V. P. Singh <sup>c</sup>, S. Sharma <sup>d</sup>, S.H. Park <sup>e\*</sup>

<sup>a</sup>*Department of Electronics and Communication Engineering, Chandigarh Engineering College, Chandigarh Group of Colleges, Jhanjeri-140307, India*

<sup>b</sup>*Department of Interdisciplinary Courses in Engineering, Chitkara University Institute of Engineering and Technology, Chitkara University, India*

<sup>c</sup>*Department of Physics, United College of Engineering and Research, Prayagraj-211010, India*

<sup>d</sup>*Department of Electronics and Communication Engineering, Indian Institute of Information Technology, Prayagraj-211015, India*

<sup>e</sup>*Department of Electronics Engineering, Yeungnam University, Gyeongsan-38541, South Korea*

This work presents a synthesis of ZnO quantum dots for white light emission for phosphors converted light emitted diodes, which is free from mixing of different luminescent QDs. The synthesis route is able to tune emission spectra from cool white to warm white light with the capability of filling the typical color gaps to replicate true spectral distribution with extraordinary fidelity and maximized the color gamut. ZnO QDs-based highly porous phosphor plate compatible for the lighting technology to maintain the individual identity of QDs is presented along with the demonstration of white LEDs from cool to warm white light.

(Received December 13, 2024; Accepted March 14, 2025)

Keywords: ZnO QDs, Co-precipitation technique, Warm white emission, Phosphors

### 1. Introduction

A quantum dot is a finest material system with extraordinary luminescence properties, also termed as artificial atom. These widely applicable nano-particles are synthesized by many ways with different pros and cons such as tuning of sharp emission with size and surface modification, solution processability, maintaining good luminescence quantum yield etc. QDs performance has been greatly improved through several innovations by core-shell structures and co-doping, donor/acceptor system schemes from visible to infrared applications. These materials have gained excellent rating over their counterpart of organic materials by reduced non-radiative decay [1]. Colloidal form of quantum dots has reached to most popular state with additional advantage for biological field in combination with many methods such as dispensing, printing and transfer, pulsed spray, and mist coating [2]. However, QDs systems are still limited for LEDs because of many physical reasons; such as side effect of host material and reabsorption issues [3].

Increasing interests of QDs as energy convertor for phosphor-converted light-emitting devices (pc-LEDs) established a domain of QDs phosphors plate with broad range of lighting application having excellent stability, luminescence efficiency, color purity, porosity, and thermal stability. However, many systems like single crystalline phosphors, glass phosphor plate, phosphor ceramic plate and different polymer matrix have been demonstrated along with different luminescent QDs for solid state lighting. All these are limited with different issues such as environmental, manufacturing, cost, thermal stability, color purity and etc. [4]. However, degradation of luminescence quantum efficiency of colloidal QDs (CQDs) is also a major concern during the process of solidification through aggregation on the edge of droplet because of diminishing the individual identity as a luminescence center [5].

---

\*Corresponding author: sihyun\_park@ynu.ac.kr  
<https://doi.org/10.15251/JOR.2025.212.177>

Subsequently, blending of different phosphors for white light faces issue of non-radiative decay of excitons through the surface states and Forster transfer, which degrades the color rendering and color temperature with time and exposure intensity [6]. To avoid such down-hill process, four-quadrant based phosphors plates are demonstrated with additional advantage of reduced re-absorption [7]. The porosity of a phosphor plate is also major factor to influence the efficacy and color quality by controlling the transmission of excitation wavelength and heat dissipation capability. Pore size engineering has already demonstrated for better thermal stability of phosphors including stable color rendering and luminous efficacy [8]. The chemical and mechanical state of this host matrix found quite sensitive for luminescence ions with crystal field distribution and phonon energy. Few efforts have been made to match this performance and functionality in this regard but still limited to achieve for good thermal stability and luminous efficacy with user friendly majors. In continuation of it, the demonstration of liquid QDs based LEDs has been taken place for maintaining the high luminescence quantum yield (QY) for dispersed condition [9]. Moreover, soft template of QDs also reported with an inorganic-organic composite in supramolecular gels and nano-fibrillar networks to maintain good photostability and luminescence properties for solid-state lighting [10]. Without any environmental challenges, different QDs phosphor systems have reported with metal oxide and nitride including perovskite with these polymer matrices along with some issues such as wide applicability and emission tuning ability [11].

Except the lighting application, a typical display screens mixed narrow RGB spectra to generate a wide shade of colors. This concept is lacking to cover some part of color gamut by missing real cyan and yellow colors. However, mixing present QDs might be able to fulfill these gaps by mixing 6 colors QDs [12]. Moreover, the wide emission spectrum may also help to achieve the good color perception by human eyes for better discrimination of the images. This effect may be reaches to worse limit narrower RGB spectrum for eye visual perception created by cone cells in the brain. Therefore, a broad emission of white spectrum might be better option in compare to the combination of narrow RGB spectra in display screen and lighting with better CRI and luminous efficacy.

Hence, this work presents a novel one step synthesis process for ZnO quantum dots for white light emission to avoid mixing of different luminescent QDs. The synthesis scheme able to tune emission spectra from cool white to warm white light with the capability of filling the typical color gaps to replicate true spectral distribution with extraordinary fidelity and maximized the color gamut. Further, we have designed a ZnO QDs-based highly porous phosphor plates compatible for the lighting technology to maintain the individual identity of property of the QDs just like a scaffold matrix. Finally, study is demonstrating white LEDs from cool to warm white light extensively with good quantum efficiency and thermal stability. Present phosphor plate system expected to reduce thermal budgets in compare to conventional host matrix of active luminescence ions, which are commonly synthesized by high pressure and high temperatures along with the compatibility of Laser diode based light source.

## **2. Methods and materials**

ZnO QDs synthesized by using a co-precipitation technique by varying  $[Zn]/[LiOH]$  molar ratio in Oleylamine. Typical synthesis resulted a size tunable defect rich ZnO QD for white emission. Synthesis endorses the different vacancies and interstitials sites on the surface including Zn amine group complexation. A phosphors plate was prepared by a quantum dot loading to a hydrogel film [13]. Further 365 nm UV chip is used to demonstrate a white light emission.

## **3. Results and discussion**

Figure 2 show the TEM micrographs for as synthesized ZnO QDs. All three synthesized ZnO QDs are found uniform spherical shape along with high crystallinity and a hexagonal wurtzite structure as revealed from inset selected area electron diffraction (SAED) pattern, which shows

perfectly visible eight diffraction rings indexed as (100), (002) (101), (102), (110), (103), (200) and (112). Corresponding histograms are also shown in below figures, which reflect an increment in average diameter from 4.5 to 6 nm. This increase in QDs size might be occurring due to increase in Zn to OH molar ratio during synthesis route.

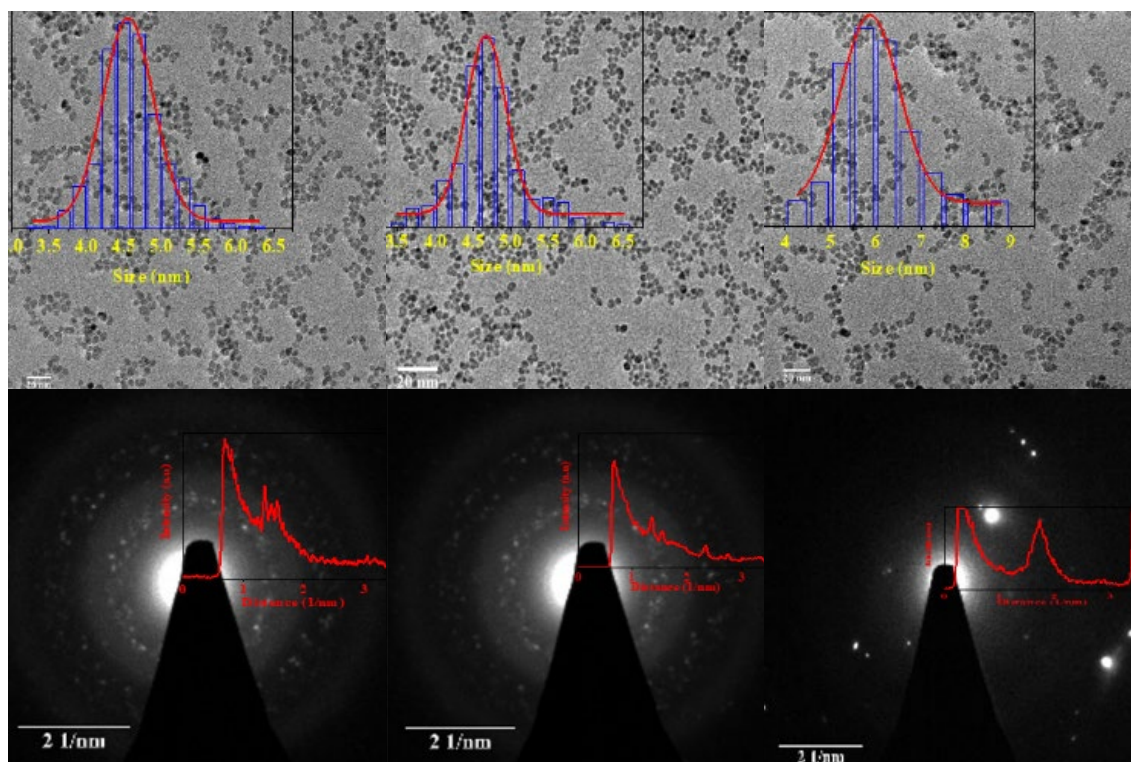


*Fig. 1. TEM analysis for different samples for ZnO QDs.*

X-ray photoelectron spectroscopy (XPS) measurements shown in fig. 2 for all synthesized ZnO QDs with different conditions to check the chemical state of different constituent atoms for examining the role of different defects and complexes in the luminescence performance along with careful relative explanation. The proposed synthesis process effect has been studied by the deconvolution of high-resolution spectra of Zn, Li, and O using Lorentzian-Gaussian fitting and subtracting the Shirley background. Fig. 2 (a, b, c) shows the Zn 2p<sub>3/2</sub> core spectra for samples S1, S2, and S3 respectively. These asymmetric peaks have been deconvoluted in three components with the electron binding energy around 1019, 1021 and 1022 eV. There is slight shifting in binding energy (BE) also observed with respect to every sample which might be because of different level of quantum confinement and chemical environment around the chemical state of the species specially with the loss of oxygen, which shift the binding state of Zn. The most intense and center feature at 1021 eV is expected to oxidation state and attributed to the Zn<sup>2+</sup> ion array surrounded by O<sup>2-</sup> ions in the hexagonal ZnO. This feature dominates over the other peaks for the all-samples data therefore it can be concluded the mostly Zn are present in doubly oxidation state. The feature towards the higher binding side around at 1022 eV is anticipated as the Zn vacancy, which signifies the formation of non-stoichiometric ZnO. The intensity of peak around 1022 eV is found to increase from sample S1 to S3, which ascribed the increasing non-stoichiometric nature especially on the surface of ZnO QDs which support the TEM result for the formation of lower index amorphous shell. The weaker intensity peak at lower BE peak around 1019 eV might be related to Zn with large dangling bond. The small sizes of QDs are expected to have this kind of features with the presence of dangling bond on non-stoichiometric surface. It has to be noticed that zinc cations are present in tetrahedrally coordinated with four oxygens and represent no broken

bond in the bulk state. The surface of nano-particles is highly imbalance for chemical species with different vacancies (oxygen vacancies in ZnO), which is expected to lower the binding energy of counterpart ions. As long as the number of broken bonds related to oxygen get increased, the amount of charge transfer from zinc cation to oxygen anion diminishes which is further lowered the binding energy significantly. Hence the feature of Zn2p<sub>3/2</sub> around 1019 eV is confirmed as Zn cation with broken bonds of oxygen anion. This consideration also expected to found substantial oxygen vacancy which will further discuss with O1s peak. A comparative analysis presented by relative concentration of different chemical of Zn2p in fig. 2d. The concentration of Zn<sup>2+</sup> oxidation state is found to be decrease from sample S1 to S3. Obviously, the reverse trend observed for the Zn vacancy concentration. However, Zn with high dangling bond did not show a fix tendency.

Analysis of Auger transition with XPS measurement provides extra degree of freedom to examine the broader chemical states of constituent atoms which deals unique kinetics with three electrons induced many body effects, which do not cover with Zn2p. This analysis also provides any minor shape change against the reference peak. Fig. 2 (e, f, and g) presented the Auger Zn L3M4.5M4.5 for sample S1, S2 and S3 respectively. All sample peak found asymmetric towards the lower BE side and deconvoluted into two features. Intense higher BE feature are attributed to oxygen bonded to metal (Zn–O) counterpart, which signifies the major presence of Zn oxidation state (ZnO). Another lower BE peak accredited to the interstitial Zn (Zn<sub>i</sub>). The BE of Zn–O bond are found consistently moved from 497 eV (S1) to 498 eV (S2) and 499 eV (S3) which is systematic with the increase in size or decrease in quantum confinement as observed in TEM measurement. With the same effect BE related to Zn<sub>i</sub> also shifted from 493 eV (S1) to 494 eV (S2) and 496 eV (S3). The relative analysis shown in fig. 2h for both features show the consistent increasing and decreasing drift for Zn<sub>i</sub> and Zn–O respectively from S1 to S3. It should be noticed that Zn<sub>i</sub> found in between lattice sites, which is quite interesting feature along with Zn vacancies. The relative concentration of O<sub>i</sub> reached to maximum 20% for samples S3. This might be possible with non-equilibrium situation during reaction which was supported with the inert environment along with stirring and pH control during reaction. Hence, a lower index amorphous shell is able to form on the surface, which also supports Zn<sub>i</sub> through adsorption during reaction. Therefore, increasing this amorphous shell would promote the higher concentration of Zn<sub>i</sub>, as found in our samples. It might be concluded that the formation of Zn<sub>i</sub> can be accompanied with V<sub>Zn</sub> as found in Zn2p spectra by just suitable reaction condition.

LiOH has been used as co-precipitation agent for ZnO nanoparticles, therefore, Li1s core level of high resolution XPS scans shown in fig. 3 (a, b, and c) for sample S1, S2 and S3 respectively and analyzed through deconvolution process. Li atom identified in the cationic (Li<sub>Zn</sub>) and interstitial (Li<sub>i</sub>) chemical state in the form of substitutional and lattice intermediate sites respectively in all samples. The Li-1s peaks found asymmetric for S1 and S2 samples, however, symmetric for S3. Li1s peak for S1 and S2 deconvoluted as lower BE around at 53 eV allocated to the Li<sub>i</sub> defects and higher BE peak around 55.7 eV related to the Li<sub>Zn</sub> or Li–O bond. The Li1s peak for S3 shows only the Li substitution at Zn site. Competitive variation of both chemical states shown in fig 3(d), which represent Li substitution found increase at Zn site from sample S1 to S3, while Li occupation of interstices gets decrease.

High resolution XPS spectra of O1s shown in fig. 3 (e, f, and g) for sample S1, S2 and S3 respectively and analyzed by deconvoluted process. The O1s peak found highly asymmetric and changed the shape significantly with the variation in experimental condition because of critical modifications on the surface as observed in TEM measurement. Deconvoluted features around 530 eV pointed as stoichiometric oxygen (S<sub>O</sub>) observed to be most intense peak for S1 and S2 sample, however, S<sub>O</sub> became less prominent for S3 because of higher surface defects related to oxygen. Other deconvoluted features of O1s peaks are recognized as oxygen vacancy (V<sub>O</sub>) and interstitial (O<sub>i</sub>) around 531 eV and 532 eV respectively. These oxygen related defects dominated for sample S3 because of highly amorphous lower index surface which are extremely prone to many defects and vacancies as discussed above with the other species of XPS spectra. Relative concentration of oxygen bonded with Zn observed to decrease consistently as shown in fig. 3(h), calculated by the normalized relative area. Moreover, O<sub>i</sub> concentration gets increased and reached to 50% maximum. Relatively, V<sub>O</sub> is not found consistent but still dominated against S<sub>O</sub>. Further, it is noticed that the reduced incorporation of Li at interstitial site basically favors the adsorption of Zn and O at

interstitial sites which might be main cause of making the surface highly amorphous and low indexed.

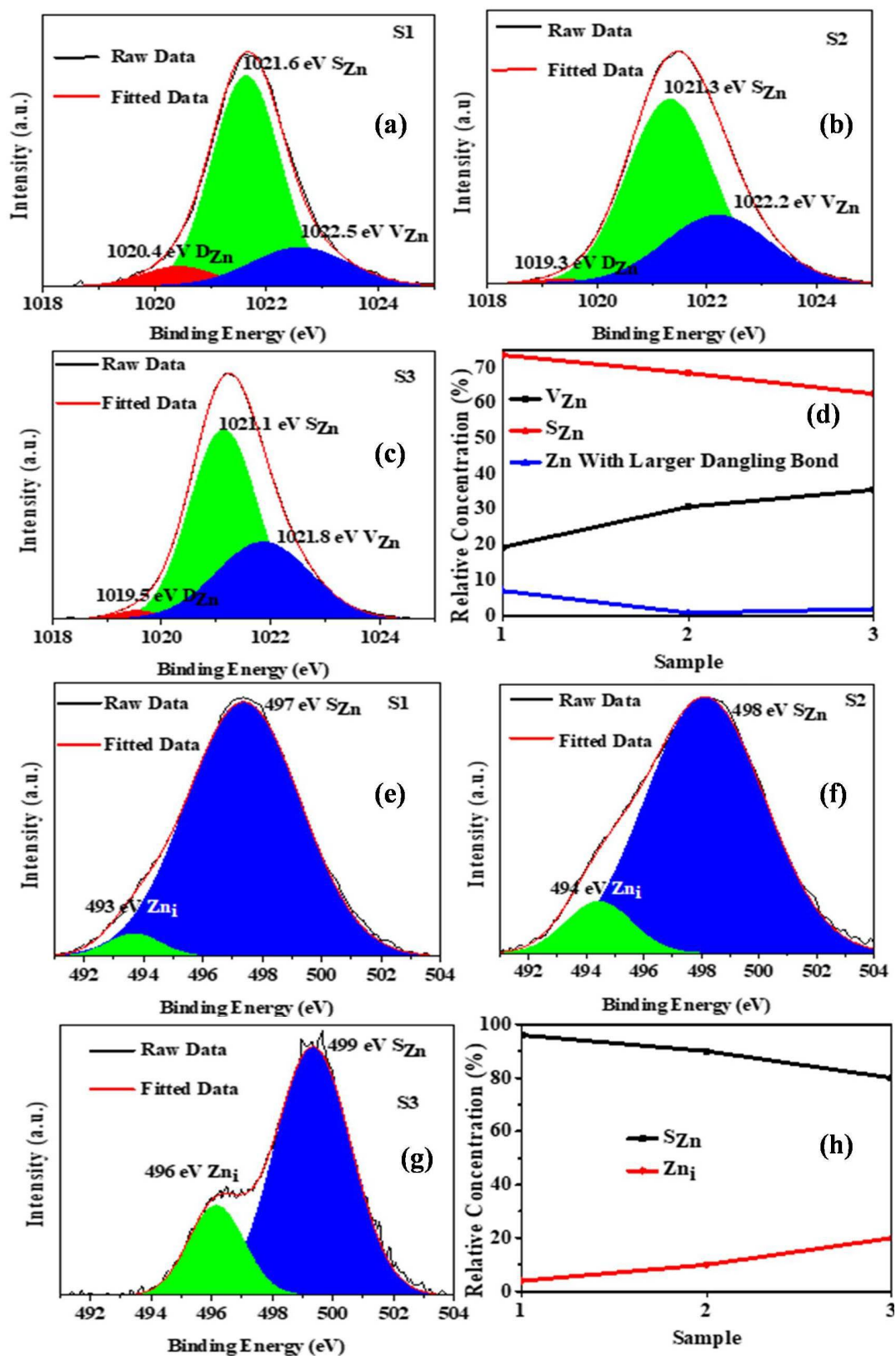


Fig. 2. XPS analysis of Zn 2p<sub>3/2</sub> and Zn Auger peak for synthesized ZnO QDs.

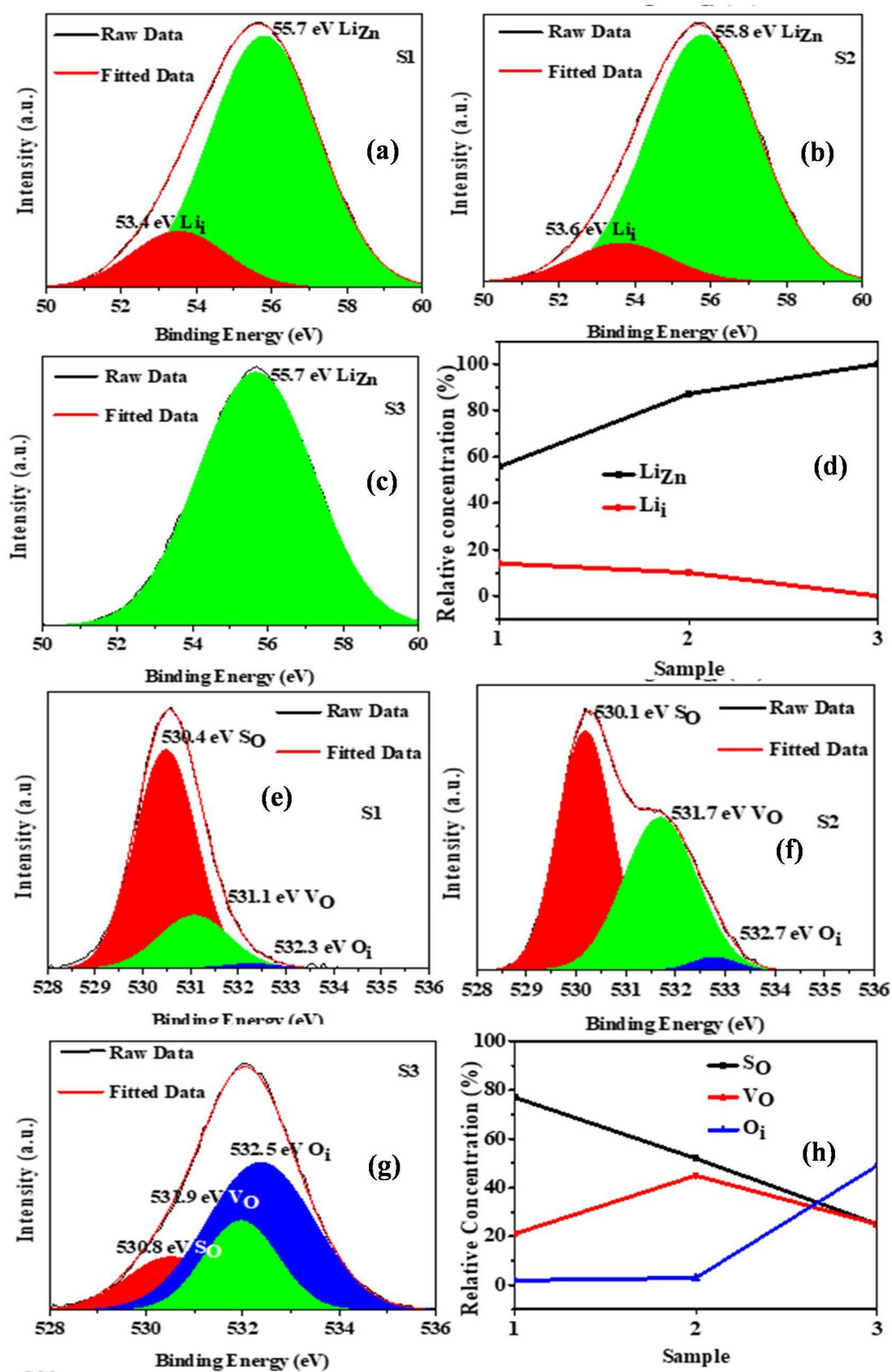


Fig. 3. XPS analysis of  $LiZn$  and  $O_{1s}$  peak for synthesized ZnO QDs.

Fig. 4 shows the absorbance, photoluminescence (PL) and time resolved photoluminescence (TRPL) spectra of synthesized ZnO QDs. Absorbance for samples from S1 to S3 found to increase in visible region which may reflect the increment in inter bandgap states induced by different surface states and interstitial sites. Corresponding PL spectrum for samples from S1 to S3 also shows increment in broad visible spectrum from yellow to orange including a tuned blue band which may shift color tone from natural white to warm white respectively. Further luminescence decay process was analyzed by TRPL spectra, which shows the shifting of luminescence towards longer time due to increment in larger surface states. Analysis reveals the three decay components as shown in figure. The decay time for first and third decay component found almost constant for all three samples. However, decay time for second component found consistently increased from sample S1 to S3. Corresponding contribution for different decay component analysis depicts in figure 4. The first decay component contribution found to decrease from samples S1 to S3 which is just reverse to the third decay component. However, second decay component contribution was not consistent.

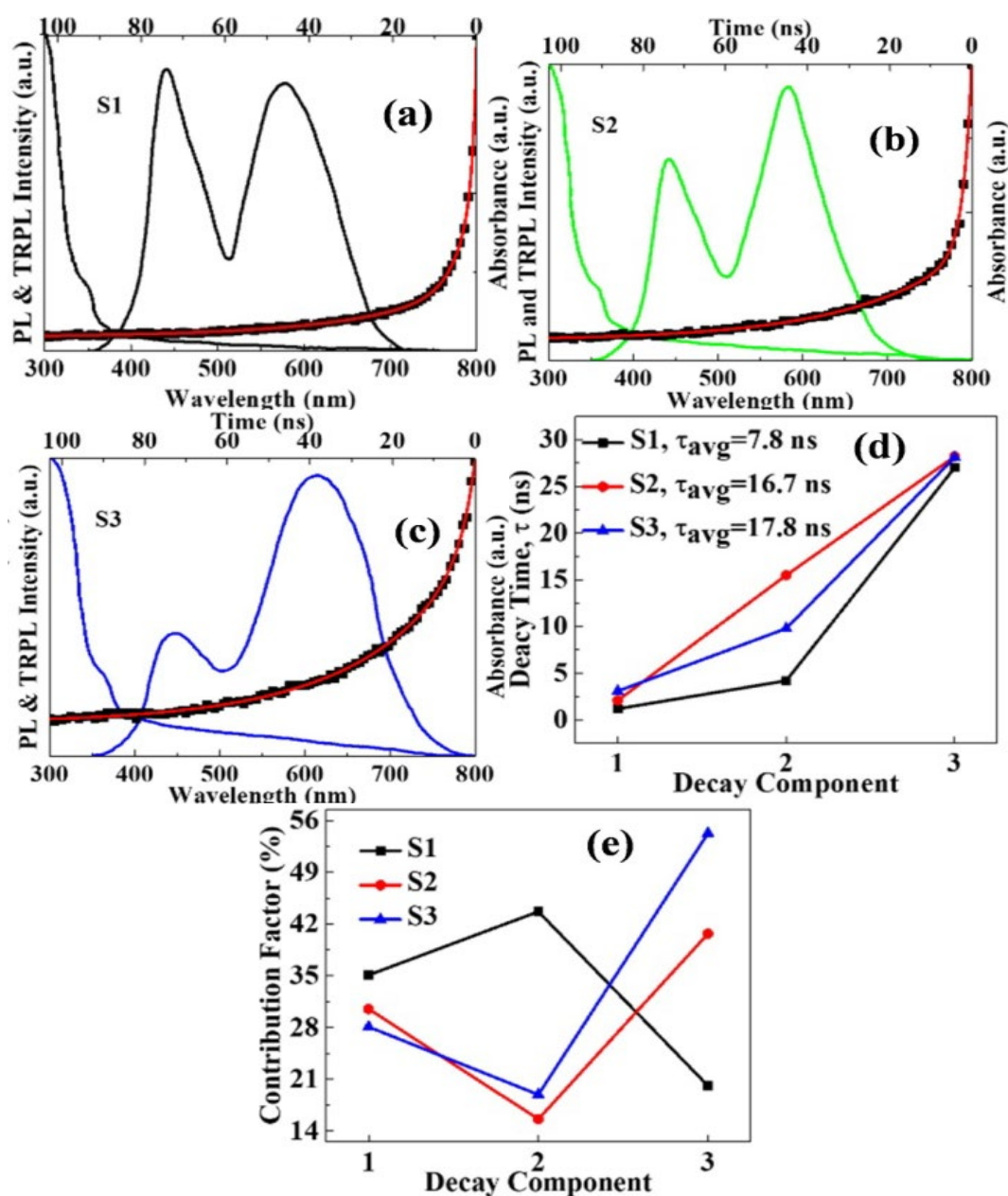


Fig. 4. Absorbance, photoluminescence and time resolved photoluminescence spectra for synthesized ZnO QDs.

Further, QDs are used to design a phosphors plate as per our previous published work [14]. Phosphors plates are used under the remote phosphor configuration. Fig. 5 shows the electroluminescence spectra for corresponding samples with corresponding correlated color temperature (CCT) and color rendering index (CRI). S3 sample shows the shift of reasonably good CRI (~86) with warm white light (CCT~2766).

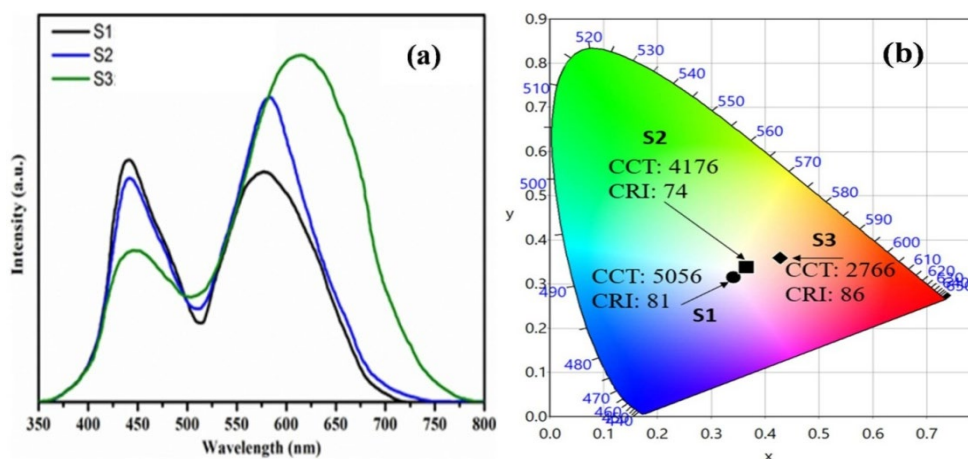


Fig. 5. Electroluminescence measurement for different samples phosphors plate.

#### 4. Conclusion

Study demonstrates ZnO Quantum dot phosphors converted LEDs to produce cool white light to warm white. The proposed design might offer new direction to use quantum dots suitable for various high-quality lighting applications.

#### References

- [1] C.W. Sher, C.H. Lin, H.Y. Lin, C.C. Lin, C.H. Huang, K.J. Chen, J.R. Li, K.Y. Wang, H.H. Tu, C.C.Fua, H.C.Kuo, *Nanoscale* 8, 1117-1122 (2016); <https://doi.org/10.1039/C5NR05676D>
- [2] Z. Gan, L.Liu, L. Wang, G. Luo, C.Moc, C.Changa, *Phys. Chem. Chem. Phys.* 20, 18089-18096 (2018); <https://doi.org/10.1039/C8CP02069H>
- [3] S. Chatterjee, U. Maitra, *Nanoscale* 8, 14979-14985 (2016); <https://doi.org/10.1039/C6NR03741K>
- [4] X. Yan, Y. Cui, Q. He, K. Wang, J. Li, *Chem. Mater.* 20, 1522 (2008); <https://doi.org/10.1021/cm702931b>
- [5] D. Bardelang, M. B. Zaman, I. Moudrakovski, S. Pawsey, J. C. Margeson, D. Wang, X. Wu, J. A. Ripmeester, C. I. Ratclie, K. Yu, *Adv. Mater.* 20, 4517 (2008); <https://doi.org/10.1002/adma.200801812>
- [6] F. Liu, Y. Sun, Y. Zheng, N. Tang, M. Li, W.Zhonga, Y.Dua, *RSC Adv.* 5, 103428-103432 (2015); <https://doi.org/10.1039/C5RA19219F>
- [7] H.Tetsuka, R. Asahi, A. Nagoya, K. Okamoto, I. Tajima, R.Ohta, A. Okamoto, *Adv. Mater.* 24, 5333-5338 (2012); <https://doi.org/10.1002/adma.201201930>
- [8] K.K. Liu, C.X. Shan, R. Zhou, Q. Zhao, D.-Z. Shen, *Opt. Mater. Express* 7, 2682-2690 (2017); <https://doi.org/10.1364/OME.7.002682>
- [9] H. Zeng, W. Cai, Y. Li, J. Hu, P. Liu, *J. Phys. Chem. B* 109, 18260-18266, 2005; <https://doi.org/10.1021/jp052258n>

- [10] Y. Fujita, K. Moriyama, Y. Hiragino, Y. Furubayashi, H. Hashimoto, T. Yoshida, *Phys. Status Solidi Curr. Top. Solid State Phys.* 11, 1260–1262 (2014);  
<https://doi.org/10.1002/pssc.201300645>
- [11] A. Asok, M. N. Gandhia, A. R. Kulkarni, *Nanoscale* 4, 4943, 2012;  
<https://doi.org/10.1039/c2nr31044a>
- [12] R. Viswanatha, H. Amenitsch, D. D. Sarma, *J. Am. Chem. Soc.* 129, 4470–4475 (2007);  
<https://doi.org/10.1021/ja068161b>
- [13] C. H. Lee, A. J. Crosby, T. Emrick, R. C. Hayward, *Macromolecules* 47, 741–749 (2014);  
<https://doi.org/10.1021/ma402373s>
- [14] M. Kumar, A. Kumar, A. H. Makki, K. S. Seong, S. H. Park, *Materials Letters* 259, 126846 (2020); <https://doi.org/10.1016/j.matlet.2019.126846>